MARKED SET
PLEASE RETURN

CRYS 6516

TYPESET FROM AUTHOR'S DISK

Crys : 6516
Date : 17/8/97

ELSEVIER

Journal of Crystal Growth 181 (1997) 17–25

JOURNAL OF CRYSTAL GROWTH

Characterization of defect structures in magnetic liquid encapsulated Kyropoulos grown InP single crystals

H. Chung[a], W. Si[a], M. Dudley[a,*], D.F. Bliss[b], R. Kalan[c], A. Maniatty[c], H. Zhang[d], V. Prasad[d]

[a] *Department of Materials Science and Engineering, State University of New York at Stony Brook, Stony Brook, NY 11794-2275, USA*
[b] *USAF Rome Laboratory, Hanscom AFB, MA 01731, USA*
[c] *Department of Mechanical Engineering, Aeronautical Engineering and Mechanics, Rensselaer Polytechnic Institute, Troy, NY 12180, USA*
[d] *Department of Mechanical Engineering, State University of New York at Stony Brook, Stony Brook, NY 11794-2300, USA*

Received 5 December 1996; accepted 24 April 1997

Abstract

Synchrotron White Beam X-ray Topography (SWBXT) has been used as a nondestructive diagnostic technique for the characterization of defect structures in large wafers cut from S and Fe-doped InP single-crystal boules. Wafers cut both longitudinally and laterally with respect to the growth axis were studied in order to reveal the overall defect distribution in the boules. Studies carried out on longitudinally cut S-doped crystals enabled information to be obtained on interface shape, from the observation of growth striations, as well as defect distribution. The conditions for optimal visibility of the growth striations were determined and it was found that the morphology of the growth interface was a sensitive function of local growth conditions. The formation of extensive slip bands from peripheral regions was also observed. This indicates that large thermal stresses were generated during crystal growth leading to such significant plastic deformation processes. Studies carried out on a series of laterally sliced, Fe-doped wafers cut from the same boule revealed dislocations in well-defined fourfold symmetric distributions. A finite element thermal-elastic stress analysis was performed for an intermediate growth stage to investigate the nature of the stress which causes this fourfold distribution. The calculated excess shear stress from this analysis agrees qualitatively with the observed dislocation distribution and slip system activity. The influence of an applied magnetic field on precipitate distributions in InP boules was preliminarily studied by examining a longitudinal cut, heavily Fe-doped InP wafer, which was grown in the presence of an intermittent applied field. Topographs recorded from this wafer revealed that no formation of large precipitates was discernible in either the initial or intermediate growth stages when the magnetic field was applied. On the other hand, the formation of large precipitates was observed in regions near the final stage of crystal growth when the magnetic field was turned off. Further such investigations are underway.

PACS: ■

Keywords: X-ray topography; InP; Growth striations; Slip bands; Dislocations and twins

* Corresponding Author: Fax: (516) 632-8052; e-mail: mdudley@ccmail.sunysb.edu.

0022-0248/97/$17.00 Copyright © 1997 Elsevier Science B.V. All rights reserved
PII S0022-0248(97)00271-6

1. Introduction

InP is an important semiconductor material for long-wavelength optoelectronic devices and high-frequency electronic devices. The performance of these devices is controlled by the structural and chemical uniformity of the epitaxial layers, which in turn, is strongly dependent on the structural perfection and compositional homogeneity of the substrates. It is, therefore, imperative to improve the crystalline quality and homogeneity of InP substrates. However, the relatively low yield stress of InP [1] makes it susceptible to deformation by stresses generated during crystal growth. It is, therefore, difficult to produce InP crystals with low dislocation density. On the other hand, temperature fluctuations imposed by turbulent convective flow give rise to uncontrolled variations in the local solidification rate and diffusion layer thickness, leading to microscopic and macroscopic chemical inhomogeneity. Improvements in the structural perfection of InP crystals has been demonstrated by using the magnetic liquid encapsulated Kyropoulos (MLEK) growth method [2]. The use of a magnetic field can dampen out the turbulent convective flow to improve the microscopic homogeneity of the crystal [3]. On the other hand, with the Kyropoulos process, where the solid–liquid growth interface is several millimeters below the encapsulating layer, the thermal stresses generated during growth can be reduced. A decrease of the dislocation density in GaAs crystals by using the liquid encapsulated Kyropoulos (LEK) growth method has been reported [4].

Defects in InP have been studied by means of optical microscopy (OM) of the etched surface [5], transmission electron microscopy (TEM) [6], and X-ray topography [7]. While OM is a quick and easy method, it can only reveal defects which create inhomogeneities as they intersect with the sample surface, yielding very little structural or crystallographic information. TEM can give detailed structural and chemical information at atomic scales, but sample preparation is difficult and destructive. In addition, only very small regions of a wafer can be examined at a time due to the extremely small field of view. By comparison, synchrotron white beam white X-ray topography (SWBXT) [8, 9] is nondestructive, and no special sample preparation is needed. It is complementary to TEM with respect to the field of view, since it can image whole wafers up to 4 in. in diameter in a single exposure. Also it is superior to conventional X-ray topography due to its high intensity, wavelength tunability, and good geometric resolution [9]. The purpose of this study is to characterize the structure, density, and distribution of defects in MLEK grown InP crystals using SWBXT. It extends our previous work [10] and presents investigations of structural defect configurations and their distributions in the different stages of crystal growth, which enables a correlation between observed defect structures and both the growth parameters and modeling predictions. The results can provide feedback to the crystal grower to enable optimization of these growth parameters.

2. Experimental procedure

All the crystals used for this study were grown with ⟨0 0 1⟩ pulling directions by the MLEK technique, at Rome Laboratory, Hanscom AFB. The crystals had a diameter of about 2–3 in. and all appeared macro-twin free to the naked eye. In the heavily Fe-doped InP crystal (wafer B), the magnetic field was turned off during part of the pulling process to investigate the effect of magnetic field on the dopant (precipitate) distribution.

SWBXT experiments were carried out at the Stony Brook Synchrotron Topography Station, Beamline X-19C, at the National Synchrotron Light Source (NSLS), Brookhaven National Laboratory. In this study, both transmission and reflection Laue geometries are employed. In the transmission topographic experiments, crystals were oriented in the beam so that the wavelengths selected for the reflections used were around 0.45 Å, which is just above the InK absorption edge (0.44 Å), to minimize photoelectric absorption. In addition, a scanning mechanism [11] comprising both vertical and horizontal translation stages is also employed to enable single-exposure imaging of these large-size wafers. To prevent possible surface deterioration of the crystals due to prolonged exposure to the intense radiation, the longer wavelength

components of the synchrotron radiation, which are most readily absorbed, were selectively removed by employing a filter consisting of a few hundred micrometers of aluminum. All images were recorded on 8″ × 10″ Kodak SR-1 high-resolution X-ray film.

3. Results and discussion

3.1. *Wafer A (S-doped wafer)*

3.1.1. *The visibility of growth striations*

In a previous paper [10], we reported on the observation of growth interface morphology in the S-doped ($1–2 \times 10^{18}$ at/cm^3) InP crystal using SWBXT. Systematic investigation of the contrast variations in the images of growth striations reveals that the visibility of growth striations is a sensitive function of diffraction geometry. Fig. 1a and Fig. 1b are transmission X-ray topographs recorded from the S-doped InP crystal showing the contrast variations in the images of growth striations in different reflections. Growth striations are clearly visible in Fig. 1a, where the lattice planes parallel to the (0 0 1) growth interface are chosen for the reflection. In contrast, growth striations are invisible in Fig. 1b, where the lattice planes perpendicular to the (0 0 1) growth interface are chosen for the reflection. The contrast variations strongly indicate that the lattice distortion arising from dopant segregation is primarily normal to the growth front. In other words, the displacement vector associated with the growth striations is perpendicular to the interface plane so that growth striations are invisible when the reflecting planes are parallel to the displacement vector. This result clearly indicates that the choice of correct orientation of the active reciprocal lattice vector with respect to the interface plane is important to optimize the visibility of growth interfaces.

3.1.2. *The Morphology of growth interface vs. growth conditions*

The morphology of growth interfaces is clearly delineated through the observation of growth striations (Fig. 1a). A significant change in the growth interface morphology was observed when the pulling process was initiated, with bimodal shape of growth interface, comprising a convex region in the center and two concave regions near the outer surface of the crystal being developed. The likely reasons for this lie in the fact that the convective flow in the melt due to both buoyancy and the combination of crucible and crystal rotation changes when the pulling process begins [12, 13]. At this point, as the shoulder of the crystal emerges from the melt into the encapsulant, the thickness of the encapsulant above the crystal decreases as the encapsulant moves into the region between the outer boule circumference and the crucible wall.

(a)

(b)

Fig. 1. Transmission X-ray topographs recorded by using (a) $g = 0\,0\,\bar{4}$, $\lambda = 0.45$ Å and (b) $g = 2\,\bar{2}\,0$, $\lambda = 0.45$ Å from a MLEK grown S-doped InP crystal showing the contrast variations in the images of growth striations (GS).

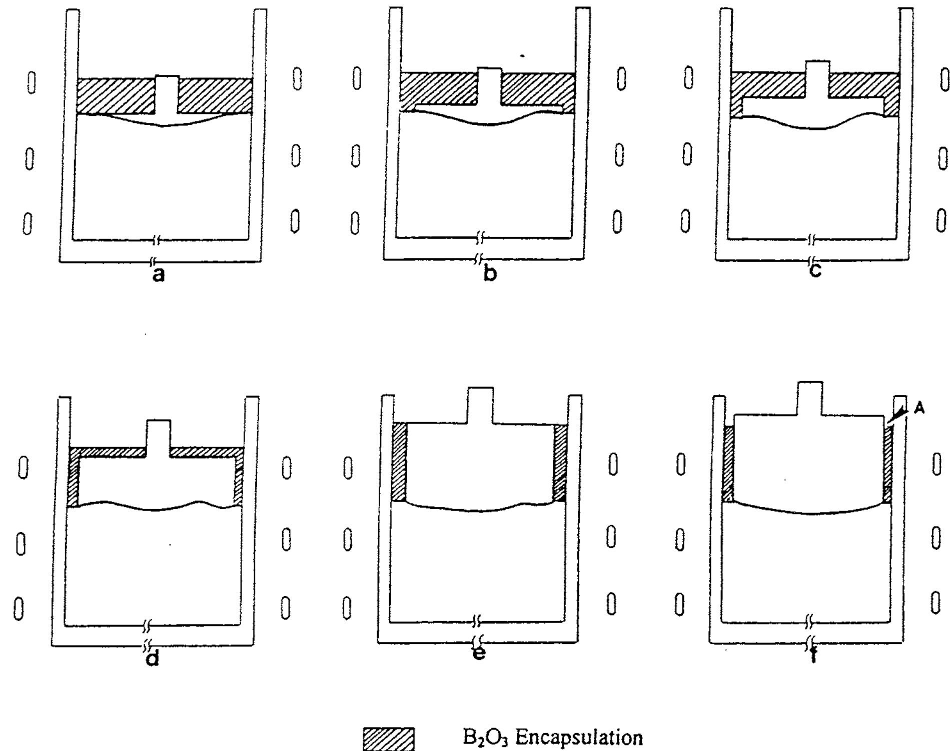

Fig. 2. A schematic diagram showing the modification of the geometric configuration of the encapsulant and the corresponding growth interface morphology observed in wafer A at the various stages of the growth process.

Fig. 2 is a schematic diagram showing the modification of the geometric configuration of the encapsulant and the corresponding growth interface morphology at various stages of the growth process. This change in the geometric configuration of the encapsulant during growth leads to a dramatic modification of the convective and radiative heat transfer from both the top and cylindrical outer surfaces of the boule. These effects modify the global heat transfer environment of the growth process and potentially cause a change in the flow pattern of the melt, which gives rise to a modification of the growth interface morphology. It is also worth noting that a well defined, slightly convex shape of growth interface was developed in the final stages of the growth process. Since the geometric configuration of the encapsulant remained the same after the flat shoulder of the boule emerged from the encapsulant, the heat transfer environment of the growth process after this point can be stable so that no significant temperature changes causing a modification of the growth interface morphology were observed in the subsequent stages of the growth.

3.1.3. The distribution of dislocations

In the growth of indium phosphide, boric oxide is used as an encapsulant to prevent the decomposition of the melt. The encapsulant also reduces the radiative heat loss from the outer surface of the crystal since B_2O_3 acts as a heat shield. The maximum heat loss, therefore, occurs at the point where the hot solid material emerges from the encapsulant (as indicated by region A in Fig. 2), which gives rise to maximum temperature gradients and thereby a large thermal stress in this region [13]. X-ray topographs revealed that the slip bands are most likely to be nucleated at this stage to relieve the large thermal stresses (Fig. 1). The diffuse

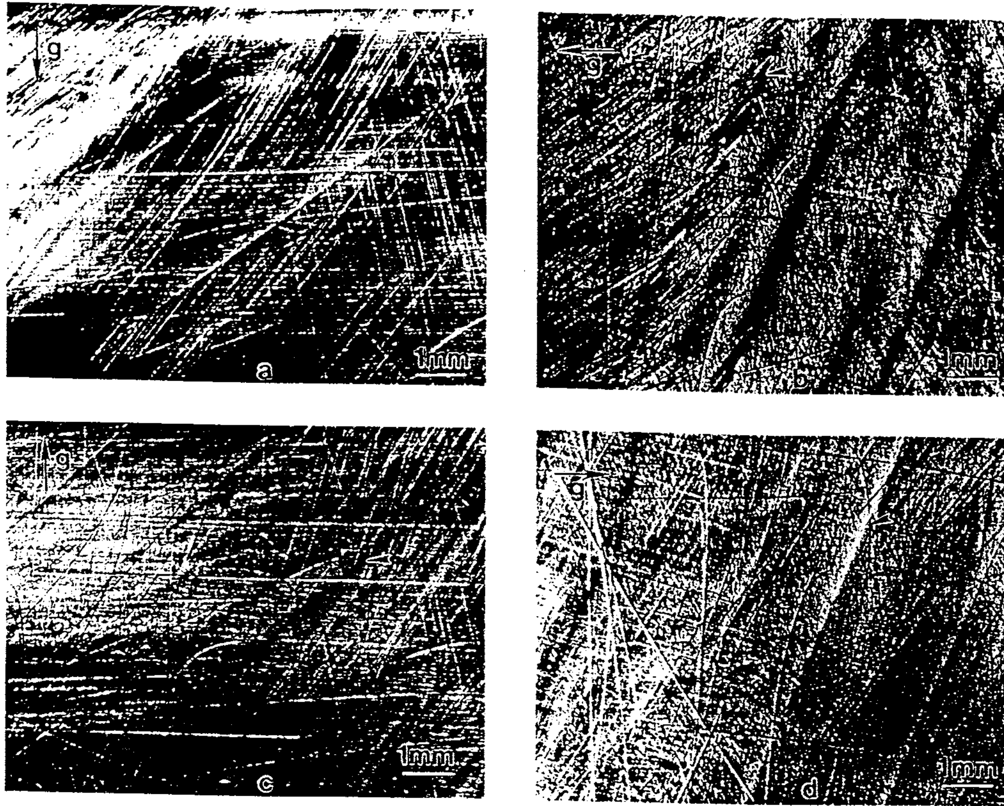

Fig. 3. Transmission X-ray topographs recorded from wafer A by using (a) $g = (1\ 1\ 1)$, $\lambda = 0.45$ Å, (b) $g = (0\ 4\ 0)$, $\lambda = 0.45$ Å, (c) $g = (1\ 1\ \bar{1})$, $\lambda = 0.45$ Å and (d) $g = (4\ 0\ 0)$, $\lambda = 0.45$ Å showing the contrast variations of a slip band.

contrast in the slip bands and in their surrounding crystal volume revealed on X-ray topographs is due to the long-range strains associated with a high density of dislocations piling up on their slip planes [14, 15]. A judicious choice of proper projection and diffraction conditions enabled individual dislocations within a slip band to be clearly resolved. Fig. 3 are transmission X-ray topographs recorded from a slip band showing the contrast variations of slip dislocations in different reflections. It is worth noting that individual dislocations are clearly visible in both (1 1 1) and (0 4 0) reflections, while only faint contrast associated with the intersection of the slip band on the X-ray exit surface can be discerned in both $(1\ 1\ \bar{1})$ and (4 0 0) reflections. The dislocation Burgers vector ($\boldsymbol{b}$) can, therefore, be determined by using the $\boldsymbol{g} \cdot \boldsymbol{b} = 0$ criterion [9], where $\boldsymbol{g}$ is the diffraction vector. The slip plane can also be determined by analyzing the projected direction and length of slip dislocations in different reflections. This slip band is, therefore, characterized to belong to the $[0\ 1\ 1]/(1\ \bar{1}\ 1)$ slip system. Systematic characterization of all the slip dislocations in this sample reveals that nine out of twelve possible $\langle 1\ 1\ 0\rangle/\{1\ 1\ 1\}$ slip systems are activated at different stages of the crystal growth process.

Calculations of the distribution of excess resolved shear stresses in the crystal at various stages in the growth process have recently been carried out by using a three-dimensional anisotropic thermo-elastic finite element model for InP single crystals. Results also confirm that the maximum excess-resolved shear stresses are generated on the outer surface of the crystal at the point where the crystal emerges from the encapsulant (see Section 3.3).

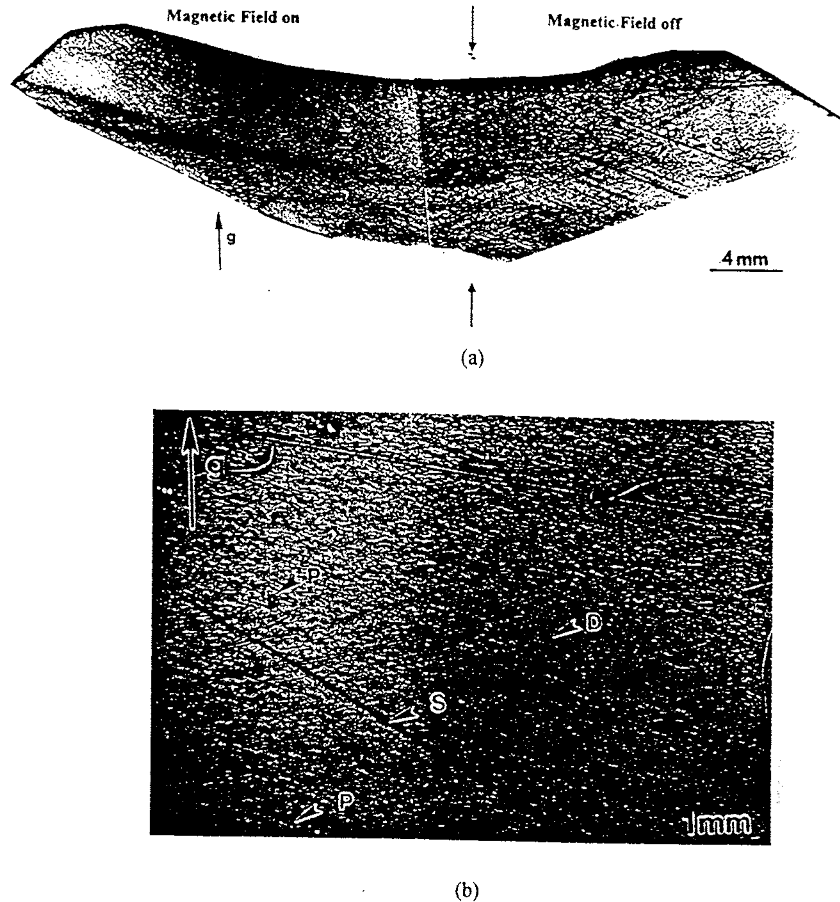

Fig. 4. (a) Reflection topographs of wafer B, $g = 4\,4\,0$, $\lambda = 0.74$ Å, which shows slip bands (S), Fe precipitates (P), and dislocation segments (D); (b) a highly magnified reflection X-ray topograph enlarged from the final growth stage.

3.2. *Wafer B (fe-doped wafer)*

In wafer B, a heavily Fe-doped (1–2×10^{19} at/cm^3) crystal, the applied magnetic field was switched off in the middle of the growth process to investigate the effect of magnetic field on dopant incorporation. The segregation coefficient of iron in indium phosphide is low (approximately 10^{-3}), so there is a strong tendency for the occurrence of macrosegregation during growth [3]. Fig. 4a is an X-ray topograph ($g = 440$, $\lambda = 0.74$ Å) recorded in reflection geometry from this sample. Images of precipitates (P) consisting of two dark, kinematic lobes positioned in the $\pm g$ directions, separated by a region of significant lattice rotation are clearly observed in the final growth stages. Fig. 4b is a highly magnified X-ray topograph recorded from this region to show the defect structures in a greater detail. It appears, therefore, that large precipitates were generated in the final growth stage when the applied magnetic field is turned off. On the other hand, no formation of large precipitates is evident in both the initial and intermediate growth stages when a magnetic field is applied. However, the presence of a very high density of dislocations in both the initial and intermediate growth stages obscured detailed observations of precipitate distributions in these regions. Therefore, studies of

dopant distributions in crystals with higher structural perfection are required to evaluate the effect of magnetic field on the homogeneity of dopant distributions in more detail.

3.3. Modeling the distribution of dislocations

The observation of dislocation distributions in a series of wafers sliced perpendicular to the [0 0 1] growth direction from a Fe-doped InP boule has been previously reported [10]. Results revealed the formation of a fourfold symmetric distribution of dislocations separated by regions of low dislocation density in the intermediate growth stages. The regions of high dislocation density are observed to lie near the periphery of the wafer along $\langle 1\ 0\ 0 \rangle$ directions, while the density of dislocations reaches a minimum along $\langle 1\ 1\ 0 \rangle$ directions. In addition, X-ray topographs recorded from wafers sliced longitudinally from MLEK grown InP crystals revealed the formation of extensive slip bands from the outer surface which have propagated into the interior of these crystals. In order to investigate the origin of the observed dislocation distributions in detail, a three-dimensional anisotropic, thermal-elastic finite element analysis of an InP single crystal at an intermediate growth stage was conducted. For a specified temperature field within the crystal, the finite element model calculates the corresponding stress field. The model incorporates room temperature values for the elastic parameters and a temperature-dependent thermal expansion coefficient. The values for three elastic parameters given by Ref. [16], are $c_{11} = 102$ Gpa, $c_{12} = 57.3$ Gpa and $c_{44} = 44.2$ Gpa. The thermal expansion coefficient for temperatures above 823 K is expressed by the following linear function [17]:

$$\alpha = 8.57 \times 10^{-9}\theta - 2.57 \times 10^{-6},$$

where θ is in Kelvin. For temperatures less than 825 K, the thermal expansion coefficient is constant, $\alpha = 4.5 \times 10^{-6}$.

The calculated stress is then projected onto the twelve primary crystallographic slip systems. This projected stress (resolved shear stress) is compared to the critical-resolved shear stress (CRSS) for a given temperature at representative points in the crystal. The temperature-dependent critically resolved shear stress for undoped InP is given by Jordan [18]. This relationship is

$$\sigma_{CRSS} = 2.133 \times 10^{5736/\theta}.$$

If the stress on the slip system at that point is less than the CRSS, then the plastic deformation will not occur in that slip system at that point. If the projected stress is greater than the CRSS then plastic slip will occur.

An analysis was carried out using the temperature field predicted by the code MASTRAPP [12]. Comparing with the experimental observations for wafer A, ten active slip systems were predicted by the model on the (1 1 1) plane. Nine correspond to those found experimentally in wafer A as summarized in Fig. 4. The tenth predicted active slip system was the $[1\ \bar{1}\ 0]/(1\ 1\ 1)$ which is symmetrically related to the $[1\ \bar{1}\ 0]/(1\ 1\ \bar{1})$ (S_9 in Fig. 1) system which was observed in the experiment.

The dislocation density is taken to be related to the total excess resolved shear stress σ^{ex} defined as

$$\sigma^{ex} = \sum_{i=1}^{N} \langle |\sigma_i| - \sigma_{CRSS} \rangle,$$

Where σ_i is the resolve shear stress on slip system i, N is the number of slip systems and the angle bracket indicates a singularity function. Fig. 5 a shows a plot of the total excess-resolved shear stress on the (1 1 0) plane. The highest stresses are found near the outside surface, where the crystal emerges from the B_2O_3 layer. The stress distribution on the (0 0 1) plane, shown in Fig. 5b, corresponds to the 90° periodicity of the cubic structure. The excessive shear stress is highest along the $\langle 1\ 0\ 0 \rangle$ and $\langle 0\ 1\ 0 \rangle$ directions and lowest along the $\langle 1\ 1\ 0 \rangle$ directions. This agrees with the dislocation density distribution observed in laterally sliced Fe-doped InP crystals as shown in Fig. 6.

4. Conclusions

Synchrotron white beam X-ray topography has been successfully applied to the nondestructive characterization of defect structures in MLEK-grown InP crystals. The conclusions include,

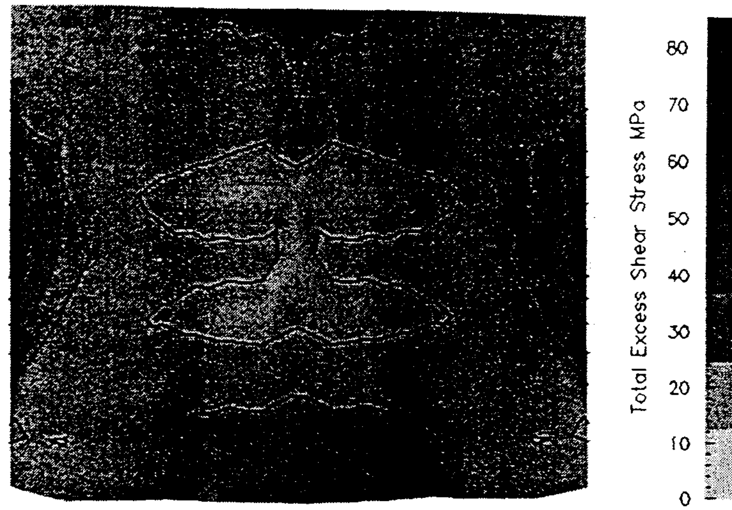

(a)

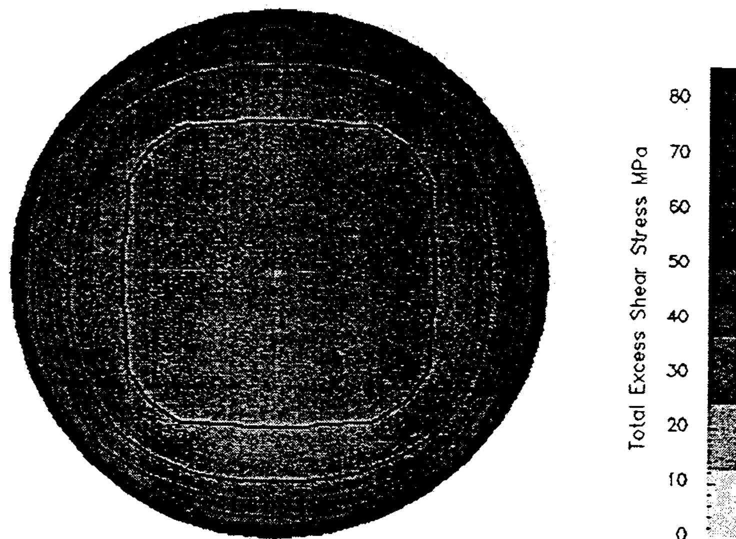

(b)

Fig. 5. (a) The distribution of the total excess resolved shear stress on the (0 1 0) plane through the center of the crystal subject to an intermediate growth stage temperature field; (b) The distribution of the total excess resolved shear stress on the (0 0 1) plane through the middle of the crystal subject to an intermediate growth stage temperature field.

1. X-ray topographs revealed that the lattice distortions associated with growth striations are normal to the growth front. The choice of correct orientation of the active reciprocal lattice vector with respect to the interface plane is important to maximize the visibility of growth interfaces.
2. The most likely origin for slip bands can be attributed to relieve large thermal stresses generated when the crystal is pulled from the encapsulant. X-ray topographic studies reveals that nine of the twelve possible ⟨1 1 0⟩/{1 1 1} systems are activated at different stages of the growth process.

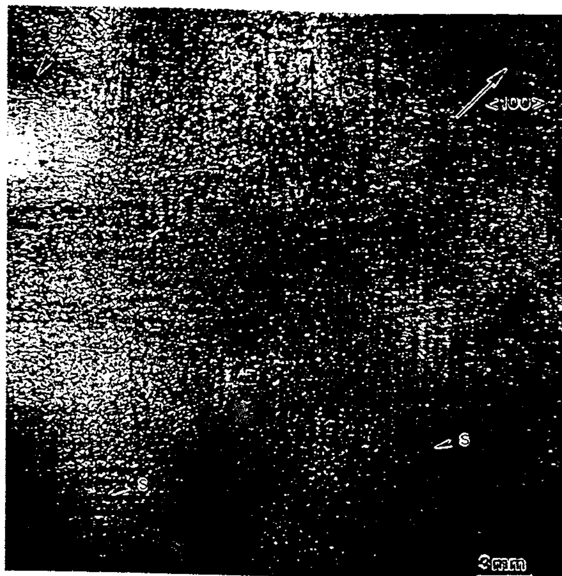

Fig. 6. Transmission X-ray topograph ($g = \bar{4}\,0\,0, \lambda = 0.45$ Å) recorded from a wafer sliced laterally from a Fe-doped InP crystal showing the fourfold symmetric distribution of dislocations.

3. Large Fe precipitates were found when magnetic field used for melt stabilization was not applied. No formation of large precipitates was discernible in both the initial and intermediate growth stages. However, the formation of a very high density of dislocations in these regions obscured a detailed observation of precipitate distributions. Studies of dopant distributions in crystals with higher structural perfection are required to evaluate in more detail the effect of magnetic fields on dopant incorporation.
4. A thermal-elastic finite element stress analysis for an intermediate growth stage shows good agreement with the observed slip system activity and with the observed fourfold symmetry of the dislocation distribution.

Acknowledgements

This work was supported by DARPA/AFOSR Consortium of Crystal Growth Research under the contract F496209510407. Topography was carried ut at the Stony Brook Synchrotron Topography Facility, Beamline X-19C, at the National Synchrotron Light Source, at Brookhaven National Laboratory, which is supported by the Department of Energy.

References

[1] M. Azzaz, J. Michel, A. George, Philos. Mag. A 69 (1994) 903.
[2] D.F. Bliss, R.M. Hilton, J.A. Adamski, J. Crystal Growth 128 (1993) 451.
[3] R.W. Series, D.T.J. Hurle, J. Crystal Growth 113 (1991) 305.
[4] G. Jacob, J. Crystal Growth 58 (1982) 455.
[5] A. Huber, N.T. Linh, J. Crystal Growth 29 (1975) 80.
[6] S. Mahajan, A.K. Chin, J. Crystal Growth 54 (1981) 138.
[7] S. Tohno, A. Katsui, J. Crystal Growth 74 (1986) 362.
[8] M. Dudley, Applications of synchrotron radiation techniques to materials science, in: D.L. Perry, R.L. Stockbauer, N.D. Shinn, K.L. D'Amico, L.J. Terminello (Eds.), Mater. Res. Soc. Symp. Proc., vol. 307, Pittsburgh PA, 1993, p. 213.
[9] M. Dudley, in: D. Bloor, R.J. Brook, M.C. Flemings, S. Mahajan (Eds.), Encyclopedia of Advanced Materials, vol. 4, Pergamon, Oxford, 1994, p. 2950.
[10] H. Chung, W. Si, M. Dudley, A. Anselmo, D.F. Bliss, A. Maniatty, H. Zhang, V. Prasad, J. Crystal Growth, 1996, in press.
[11] S. Wang, M. Dudley, W. Huang, C.H. Carter Jr, V.F. Tsvetkov, C. Fazi, in: W.M. Bullis, D.G. Seiler, A.C. Diebold (Eds.), Semiconductor Characterization Present Status and Future Needs, AIP Press, New York, 1996, p. 278.
[12] H. Zhang, V. Prasad, D.F. Bliss, J. Crystal Growth 1996, in press.
[13] Y.F. Zou, G.-X. Wang, H. Zhang, V. Prasad, D.F. Bliss, J. Crystal Growth, submitted.
[14] A. Authier, A.R. Lang, J. Appl. Phys. 35 (1964) 1956.
[15] J. Wu, T. Fanning, M. Dudley, V. Shastry, P. Anderson, Defect engineering in semiconductor growth, processing and device technology, in: S. Ashok, J. Chevallier, K. Sumino, E. Weber (Eds.), Mater. Res. Soc. Symp. Proc., vol. 262, Pittsburgh PA, 1993, p. 265.
[16] S. Adachi, J. Brice (Eds.), Properties of Indium Phosphide, INSPEC, The Institution of Electrical Engineerings, New York, 1991.
[17] V.M. Glazov, K. Davletov, A. Ya Nashel'skii, M.M. Mamedov, Russ. J. Phys. Chem. 51 (1977) 1496.
[18] A.S. Jordan, G.T. Brown, B. Cockayne, D. Brasen, W.A. Bonner, J. Appl. Phys. 58 (1985) 4383.